Monoenergetic Proton Beams from Laser Driven Shocks

Dan Haberberger, Sergei Tochitsky and Chan Joshi

University of California, Los Angeles

Abstract. Laser driven ion acceleration (LDIA) has the potential to deliver compact and affordable accelerators for applications in many fields of science and medicine. Specifically, radiotherapy of cancerous tumors requires ion energies in the range of 200-300 MeV/a.m.u. and with energy spreads on the order of 5%, parameters thus far beyond the LDIA experimental results using the most powerful lasers in the world. Recently, it was shown experimentally that laser-driven collisionless shocks can accelerate proton beams to 20 MeV with extremely narrow energy spreads of about 1% and low emittances [1]. This was achieved using a linearly polarized train of CO_2 laser pulses having a peak power of 4 TW interacting with a hydrogen gas-jet target. Motivated by these results, presented here is a systematic study of the basic physics of collisionless shock waves using 1D OSIRIS simulations. Shock formation, Mach number, and reflection of protons are key processes observed versus the initial density and drift velocity of two interpenetrating plasmas.

Keywords: Laser proton/ion acceleration, collisionless plasma shocks
PACS: 52.38.Mf, 41.75.Jv, 52.35.Tc, 52.35.Fp

INTRODUCTION

Interest in the field of laser driven ion acceleration (LDIA) has exploded over the past decade with the availability of multi-TW laser pulses. Focus in the field began the early 2000's where the interaction of the first 100 TW to PW-scale laser systems with solid foils produced a copious amount of forward directed ions in the 10's of MeV/amu energy range [2, 3]. The high quality of these laser driven ion beams [4] has given rise to a host of applications. For example, laser driven proton beams can be used to radiograph strong electric fields in dense laser-plasma interactions resolving a spatial scale of 1 μm and a temporal scale of picoseconds[5]. A host of other proposed applications for LDIA beams include radiotherapy of cancerous tumors [6, 7], generation of short lived isotopes needed in positron emission tomography [8], high-brightness injectors for conventional accelerators [9], and as a fast ignitor in inertial confinement fusion [10]. Application driven requirements set for these laser-driven ion beams are high energies: 200-250 MeV/amu [6, 7]; and narrow energy spreads: $\sim$1-5% for cancer therapy [6, 7] and $\sim$1% for an injector source to conventional accelerators [11].

There are various LDIA mechanisms under study which all originate in a space-charge separation driven between the plasma electrons and ions. Here we characterize them for convenience by laser polarization (electron heating) and target thickness. By far the most studied mechanism is target normal sheath acceleration (TNSA)[12, 13]. Here, a high-power, linearly-polarized laser pulse is incident upon a thin ($\sim\mu$m scale) solid target where electrons are efficiently heated to high energies. These heated electrons traverse through the target and set up a sheath field on the back side which accelerates ions from the rear surface [14]. Though this mechanism has been used to produce 60 MeV protons, the accelerated ions typically have a characteristic exponential spectrum. Recently two groups have had limited success in obtaining a peak in the TNSA generated spectrum with a full width at half maximum energy spread $\Delta E/E_{FWHM}$ $\sim$ 20% by engineering the target geometry or composition, but the ion energies were limited to a few MeV [15, 16]. When the target thickness is decreased to 10's of nanometers, one can take advantage of the fact that the target will become relativistically transparent during the interaction. This leads to much higher coupling between the laser and the electrons allowing for an enhancement to the space-charge separation field which has yielded GeV heavy ion energies and 120 MeV proton energies (Daniel's dissertation).

Radiation pressure acceleration (RPA) is a mechanism that relies on the use of circular polarization to minimize electron heating. This allows a charage separation to build up at the front of the laser pulse by the controlled push of the ponderomotive force on the plasma electrons. Recently, the thick target regime, called hole boring, was demonstrated using a circularly-polarized, 8 ps CO_2 laser pulse interacting with a gaseous target producing 1 MeV protons with a $\Delta E/E_{FWHM} \sim 10\%$ [17, 18]. As the target thickness is decreased down to the laser skin depth, one enters the RPA light sail (RPA-LS) regime where the laser is able to accelerate all the target electrons within the focal volume which quickly accelerates the ions to high speeds. The co-propagating electron-ion-laser structure allows for an efficient

energy transfer from the laser to the electrons and then to ions producing, in simulations [19], ions in the GeV range with narrow energy spreads. Though the RPA-LS mechanism seems promising, the data is scant with the only result reported to date yielding C^{6+} ions with an energy of ∼30 MeV and a $\Delta E/E_{FWHM} \sim 50\%$ [20]. This is mainly due to few nanometer thick targets (required by this mechanism) being ionized by the laser prepulse and expanding before the main pulse arrives. Additionally, this mechanism is very susceptible to transverse laser plasma instabilities, such as the Rayleigh-Taylor instability [21], which break up the ultra thin target preventing acceleration of all the target ions.

Recently, a new LDIA mechanism has been demonstrated at the UCLA Neptune Laboratory: shock wave acceleration (SWA)[1]. Here it was shown that a train of multiterawatt CO_2 laser pulses incident upon an overdense ($n_p > n_{cr}$) hydrogen gas jet can ionize the gas creating an electron-proton plasma and launch a shock wave at the point of reflection of the incident laser pulse. This shock is observed to propagate through the expanding plasma at a constant speed and reflect protons to high velocities forming a monoenergetic proton beam. Proton energies as high as 22 MeV with an energy spread of down to 1% were obtained. These results showed a marked improvement in the peak energy and an order-of-magnitude improvement in the energy spread of proton beams obtained in both TNSA and RPA experiments. Motivated by these results, a basic understanding of shock wave physics in relativistic plasmas relevant to the experiment (∼MeV electron temperature) is presented here.

A shock wave is a disturbance that propagates through a medium faster than the velocity of a pressure wave, or sound wave. In a plasma, a shock is formed by the collision, or interpenetration, of two plasmas where a strong gradient in pressure can be created under certain conditions. The shock which forms at this pressure discontinuity then travels from the high pressure, or downstream, plasma towards the low pressure, or upstream, plasma. Due to the collective nature of the particles within a plasma, shocks can exist where collisions are not prominent. A shock is defined as collisionless if the mean free path between particle collisions is larger than the shock width. Here, the dissipation mechanism across the shock is often acceleration of upstream ions to high energies (as in the case of the gamma ray production [22, 23]).

In order to understand the basic physics behind the formation of collisionless shocks in plasmas, shocks formed from the interpenetration of two plasmas are studied via 1D OSIRIS simulations [24]. The process by which a shock is formed is studied for the case of the expansion of a dense plasma into a rarefied one [25], as well as the case where there is an initial bulk drift between the two plasma populations. Conditions under which an ion acoustic wave forms in lieu of a shock wave are also presented. The various dissipation mechanisms of proton reflection, proton heating, and electron heating are studied in detail. Finally, a relation is made between the driven shocks in the 1D simulations and the laser driven shock case.

THE FORMATION OF COLLISIONLESS SHOCKS

To investigate the characteristics of a collisionless electrostatic shock such as formation, structure, and speed, a number of simulations were run using a “halfplane" geometry. Here, two semi-infinite plasmas are placed next to one another and initialized with their respective density, temperature, and bulk flow velocity. The ensuing interpenetration of these plasmas due to either expansion and/or initial bulk flow creates a propagating wave response traveling from plasma 1 (left or downstream side) towards plasma 2 (right or upstream side). The simulations have the following parameters : box size of 1500 (c/ω_p) or 8004 cells, initial border between the plasmas at 600 (c/ω_p), 256 particles per cell, and a time step of dt = 0.1874 ($1/\omega_p$). The simulations use an electron-proton plasma representing ionized hydrogen.

The simplest case to examine is where plasma 1 is initialized with a higher density and therefore expands into plasma 2 with no initial drift velocity. In the absence of plasma 2, the process of ambipolar diffusion occurs causing expansion of plasma 1 into vacuum with the characteristic velocity C_s [26], the sound speed. This expansion is driven by an electric field set up at the plasma-vacuum interface by the electrons in the tail of the Maxwellian velocity distribution function. These electrons create a space charge separation as they leave the slower ions behind. This ‘expansion field’ holds back the bulk of the electrons to a sheath that extends beyond the ion density with a characteristic scale length of the Debye length, λ_{De}. The introduction of plasma 2 does two things. First, electrons in plasma 2 are able to stream into plasma 1 partially compensating for the space charge separation set up by the ambipolar diffusion of plasma 1, therefore decreasing the electric field and speed at which it propagates. Second, the remaining expansion field due to the density drop that propagates into plasma 2 can drive an IAW or shock wave depending on the speed at which it propagates. Alternatively, one can initialize the plasmas with a bulk flow velocity such that they are set to collide at t = 0 with a relative velocity, V_d. Here, a shock will form in the same manner as described above but now the expansion field is driven into plasma 2 at a higher velocity. These ‘driven shocks’ can be formed with equal densities in both plasmas because the plasmas will overlap due to the relative velocity forming a density step.

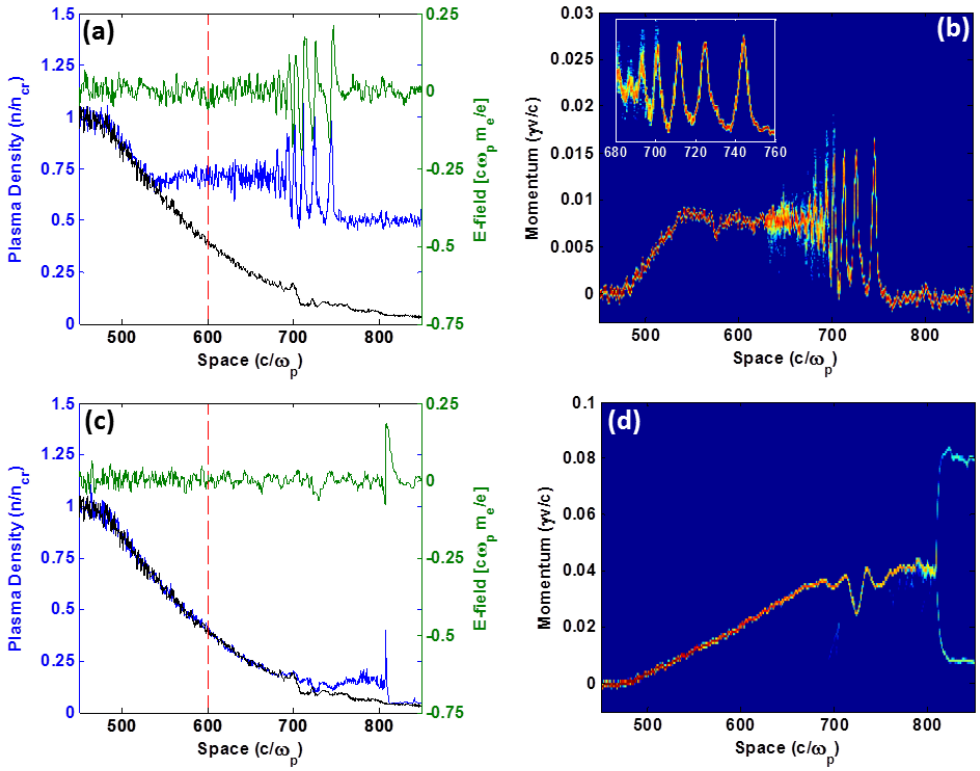

FIGURE 1. The results at a time of t = 4,722 ($1/\omega_p$) of the expansion of a dense plasma initialized at $x/\omega_p < 600$ into a less dense plasma initialized at $x/\omega_p > 600$. The density ratios are $\Gamma = 2$ (a,b) and $\Gamma = 40$ (c,d). The proton density (blue lines) and the longitudinal electric field (solid green lines) are plotted versus space for $\Gamma = 2$ (a) and $\Gamma = 40$ (c) where the dashed red line represents the initial boundary between the two plasmas. The proton density is compared to that without plasma 2 where plasma 1 simply expands into vacuum (black lines). The proton longitudinal phase space is plotted for $\Gamma = 2$ (b) and $\Gamma = 40$ (d). There is no relative drift between the plasmas, $V_d = 0$, the protons are initialized cold ($T_i = 10$ eV), and the initial electron temperature is $T_e = 770$ keV ($C_s = 0.0286c$).

These concepts are displayed in Fig 1 which displays a snapshot of the proton density (a,c : blue lines), longitudial electric field (a,c : solid green lines), and proton longitudinal phase space (b,d) for an initial density ratio of $n_1/n_2 = \Gamma = 2$ (a,b), and similarly for $\Gamma = 40$ (c,d). The snapshots are taken at a time of 4,722 ($1/\omega_p$), where ω_p is the plasma frequency at $n/n_{cr} = 1$). There is no relative drift between the plasmas, $V_d = 0$, and the initial particle temperatures are $T_i = 10$ eV and $T_e = 770$ keV ($C_s = 0.0286c$). The proton densities in Fig. 1a and b shown in blue lines are compared to that for expansion in vacuum ($n_2 = 0$) shown in the black lines. The red vertical line at $c/\omega_p = 600$ shows where the initial boundary between plasma 1 and 2 was at t = 0. In both cases, the characteristic rarefaction wave associated with plasma expansion into vacuum can be seen at x = 470 (c/ω_p) traveling in the negative x direction at 0.0275c ($\sim C_s$), in good agreement with theory [27]. In the case of $\Gamma = 2$ where the plasmas have similar densities, plasma 2 has impeded the expansion of plasma 1 into vacuum at a high density ($n \sim 0.75n_{cr}$) where the expansion velocity is $\sim$0.009c ($0.31C_s$). This can be seen from Fig. 1b in the range from $c/\omega_p \sim$ 500-550 where pure expansion is taking place achieving a maximum velocity of $\sim$0.009c before a plateau is created due to the presence of plasma 2. Such a sub-sonic disturbance is seen to launch an IAW into plasma 2 traveling at an observed velocity of 0.031c ($1.08C_s$), slightly above the sound speed. The IAW is characterized by a bunching of the ions seen in the density (Fig. 1a), an oscillatory electric field (Fig. 1a), and an oscillatory modulation of the momentum seen in the proton phase space (Fig. 1b).

In contrast, the case of $\Gamma = 40$ presented in Fig. 1c and d shows very different results. Here, plasma 2 impedes the expansion of plasma 1 at a density of $\sim 0.2n_{cr}$ where the expansion velocity is far above the sound speed, $\sim$0.04c = $1.4C_s$ (see Fig. 1d). At this speed, a shock has been launched traveling at a supersonic speed of 0.044c ($1.54C_s$). The shock is characterized by a single spike in the proton density and electric field (Fig. 1c), and full reflection of the upstream protons (Fig. 1d). Reflection of protons from the moving potential associated with the spike in the electric

field results in proton velocities of :

$$V_{refl} = 2V_{sh} - V_{up} \tag{1}$$

where V_{refl}, V_{sh}, and V_{up} are the velocities of the reflected protons, the shock, and the upstream protons, respectively. This equation is easily understood by comparison to a ball bouncing off a moving wall. As seen in Fig. 1d, for the observed V_{sh} = 0.044c and V_{up} = 0.008c, the reflected protons travel at a velocity of V_{refl} = 0.08c in full agreement with Eq. 1. These two examples of Γ = 2 and Γ = 40 represent two extreme cases of launching an IAW and a pure shock wave with full reflection. For the cases with Γ that lie in between 2 and 40, many interesting, yet complicated, phenomena occur such as partial proton reflection, proton heating though the shock, and proton trapping behind the shock. The resulting structure appears as a shock followed by a decaying wave structure similar to an IAW.

Many of these phenomena, and the transition between them, can be observed in the proton longitudinal phase space by varying Γ for the expansion shocks or varying V_d for the driven shocks. Fig. 2 displays the resulting proton phase spaces in the driven case at t = 3,972 ($1/\omega_p$) for an initial V_d equal to 0.02c (a), 0.03c (b), 0.04c (c), 0.06c (d), 0.10c (e), and 0.16c (f). For all cases, the electron temperature is T_e = 511 keV (C_s = 0.0233c). The color scale is logarithmic to highlight the trapped and reflected proton populations. Though Γ = 1 in all these cases, the overlap of the two plasmas caused by their initial relative drift velocity causes the formation of a sheath field similar to that in the expansion case. At a small V_d = 0.02c (Fig. 2a), an IAW has formed similar to that in Fig. 1b in the expansion case. As V_d increases, the potential within the wave increases and begins to trap protons as seen for V_d = 0.03c (Fig. 2b). Further increase of V_d to 0.04c (Fig. 2c) shows the onset of proton reflection from the leading edge of the wave. Also seen here is the clear separation of longer wavelength (smaller k, where k is the wavenumber) modes of the wave due to dispersion. From this point when reflection begins, increasing V_d (Fig. 2d,e) increases the proton reflection and the trailing waves begin to be strongly damped due to trapping which heats the transmitted protons. Finally, if V_d is increased enough, the plasmas simply pass through one another with very little interaction as shown in Fig. 2f for V_d = 0.16c.

To summarize, the response of a plasma due to a propagating sheath field, or potential, involves the formation of a wave-like structure. This moving potential can be the result of the expansion from an initial density discontinuity between two plasmas or from an initial relative drift velocity. For small values of Γ ($\sim$2) in the expansion case or a small initial drift velocity ($V_d \leq C_s$) in the driven case, an ion acoustic wavetrain is formed. By increasing Γ or V_d the onset of proton trapping and eventually proton reflection from the leading peak of the wave is observed. These processes will be examined in more detail in the following section.

DISSIPATION OF SHOCK ENERGY

By definition, there must exist a pressure difference between the upstream and downstream plasmas across a shock which is characterized by a change in the density and/or temperature. As a shock propagates, the change in the state of the plasma represents a form of energy dissipation. This can be easily accomplished by collisions within the shock, though this will be shown to be not the case in the parameter space analyzed here.

Particle Collisions in Hot Plasmas

The three possible binary collisions are electron-electron, electron-ion, and ion-ion. For these to play a part in the shock dynamics, the mean free path of a particle in between collisions (λ_{e-e}, λ_{e-i}, λ_{i-i}) must be on the order of or smaller than the shock thickness. For the collision calculations, we choose a plasma density $n_p = 10^{19}$ cm^{-3} which is typical for a gas jet target in laser produced plasmas. Using this density, the thickness of the shock shown in Fig. 1c and d is approximately 16 μm (10 c/ω_p). The collision frequencies for the three binary collisions and their corresponding mean free paths can be calculated according to the following engineering formulas [28, 29] :

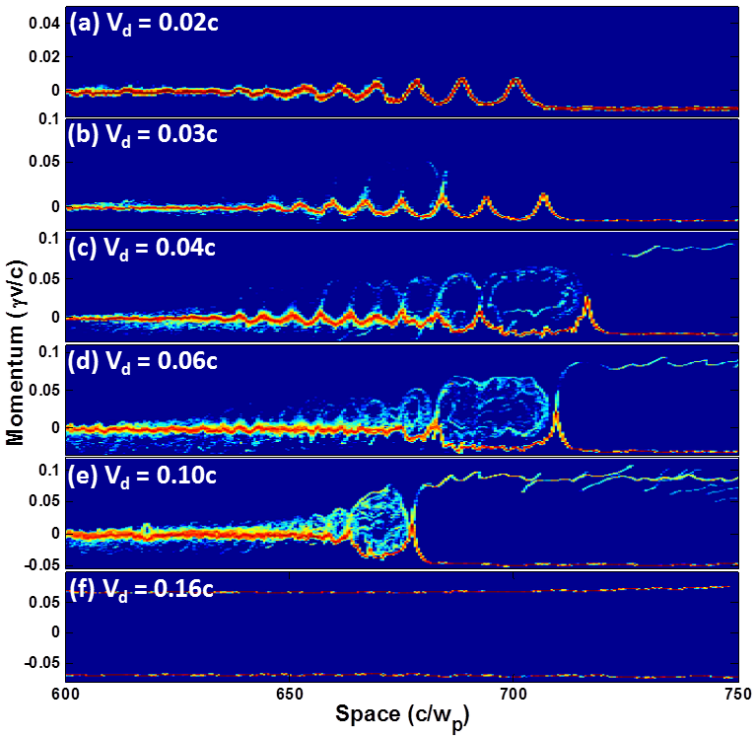

FIGURE 2. Proton longitudinal phase spaces plotted in the driven case at t = 3,972 ($1/\omega_p$) for an initial V_d equal to 0.02c (a), 0.03c (b), 0.04c (c), 0.06c (d), 0.10c (e), and 0.16c (f). The simulations are run in the center-of-mass frame, therefore plasmas 1 and 2 have an initial velocities of $V_d/2$ and $-V_d/2$, respectively. The protons are initialized cold (T_i = 10 eV) and the electron temperature is T_e = 511 keV and the initial boundary between plasmas 1 and 2 is at c/ω_p = 600.

$$\nu_{e-e} = 5 \cdot 10^{-6} \frac{n_p ln(\Lambda)}{T_{e,eV}^{3/2}} \qquad \lambda_{e-e} = \frac{v_{th,e}}{\nu_{e-e}} \tag{2}$$

$$\nu_{e-i} = 2 \cdot 10^{-6} \frac{Z n_p ln(\Lambda)}{T_{e,eV}^{3/2}} \qquad \lambda_{e-i} = \frac{v_{th,e}}{\nu_{e-i}} \tag{3}$$

$$\nu_{i-i} = 5 \cdot 10^{-8} Z^4 \sqrt{\frac{M_p}{M_i}} \frac{n_p ln(\Lambda)}{T_{i,eV}^{3/2}} \qquad \lambda_{i-i} = \frac{v_{th,i}}{\nu_{i-i}} \tag{4}$$

where Z is the ionization state, M_p is the mass of a proton, M_i is the mass of the ion, and ln(Λ) is the Coulomb logarithm assumed to be 10. For collisions including electrons, their highly relativistic temperature of 1.5 MeV combined with gas jet densities of $n_p = 10^{19}$ cm^{-3} results in a λ_{e-e} and λ_{e-i} ($\propto T_e^2/n_e$ per Eq. 2 and 3) on the order of 100's of meters, therefore electron collisions play no part in the shock dynamics. On the other hand, the ions are very cold and for an initialized T_i = 10 eV, $\lambda_{i-i} \sim 0.2$ μm. Therefore the ions in plasma 1 and 2 are initially collisional within their respective populations. However, the question is whether the upstream and downstream ions are collisional across the shock which is a calculation based on their relative bulk flow velocity according to the following equation: $\lambda_{i-i} = 2\pi\varepsilon_o^2 M_i^2 V_i^4 / n_p Z^4 e^4 ln(\Lambda)$, where ε_o is the permitivity of free space, V_i is the relative bulk flow velocity of the ions, and e is the charge of an electron [30]. The strong quartic dependence on V_i results in a λ_{i-i} of 100's of meters for the shock shown in Fig. 1d where $V_i \sim 0.04c$. These calculations show the clear collisionless nature of the shock.

Proton Reflection

One of the main dissipation mechanisms of collisionless shocks is the acceleration, or reflection, of upstream ions. As the ions stream into the shock region, if their initial kinetic energy in the frame of the shock, KE = $(1/2)M_i v_i^2$, is less than the shock potential, PE = $e\phi$, then the ion will be turned around due to acceleration and leave the shock region with a velocity according to Eq. 1. In this manner, the shock exchanges energy with the surrounding plasma which can decrease its potential and result in a slower shock velocity.

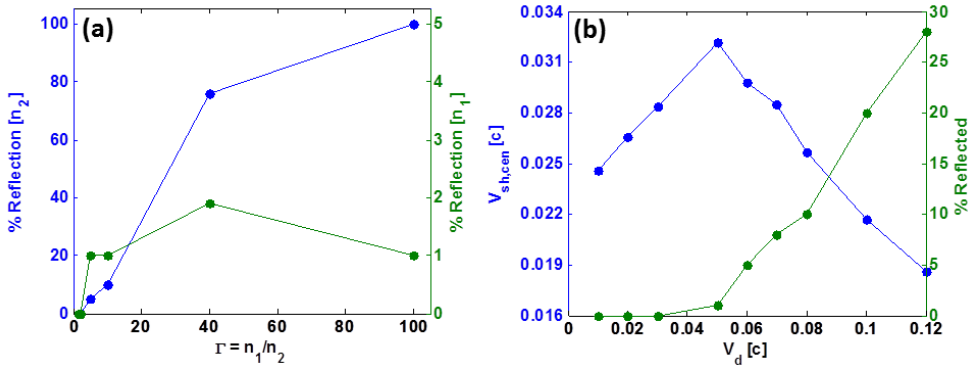

FIGURE 3. (a) The percent of reflected protons plotted versus $\Gamma = n_1/n_2$ for the expansion shock case ($V_d = 0$). The reflection is normalized to n_1 and n_2 on blue and green axes, respectively. (b) The shock velocity in the center of mass frame, $V_{sh,cen}$ (blue), and the percent of reflected protons (green) for the driven shock cases plotted versus drive velocity, V_d. The electron temperature for the expansion shock cases is T_e = 770 keV and for the driven shock cases is T_e = 511 keV. Γ = 1 for all the driven shock cases.

Fig. 3 displays the percent of protons reflected for expansion shocks versus Γ and for driven shocks versus V_d. As shown in the blue data points in Fig. 3a, the percent of protons of plasma 2 that are reflected increases from 0 at a Γ = 1.3 to 100% at a Γ = 100. However, due to the strong increase in Γ, if one normalizes the reflected particles to the density of the drive plasma (plasma 1), the peak reflection only reaches 2% indicating that the shock is not dissipating much energy. The dynamics are quite different in Fig. 3b for the case of driven shocks. For all these cases, $n_1 = n_2$ (Γ = 1) and T_e = 511 keV (C_s = 0.0233c). Here we can see the reflection begins to rise at V_d = 0.04c and reaches a peak of ∼28% at V_d = 0.12c, representing a strong dissipation of energy. Also plotted in blue is the shock velocity measured in the center-of-mass frame, $V_{sh,cen} = V_sh - V_d/2$, to isolate it from the driving speed, V_d. In this frame of reference, $V_{sh,cen}$ increases with V_d to a maximum of 0.033c then begins to fall. This peak correlates precisely to the point at which the reflection of protons becomes significant (V_d = 0.05c) indicating that the shock is losing energy to the accelerated protons.

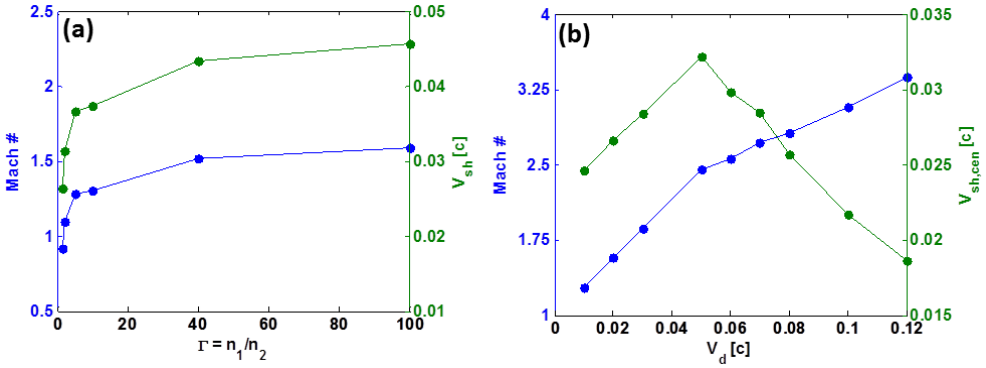

FIGURE 4. (a) The mach number and shock velocity versus Γ for the expansion shock cases (T_e = 770 keV, C_s = 0.0286c). (b) The mach number and the center-of-mass shock velocity versus V_d for the driven shock cases (T_e = 511 keV, C_s = 0.0233c).

A useful figure of merit for analyzing the speed of a shock (and ultimately the speed of reflected ions) for a given electron temperature, or sound speed, is the Mach number. It is defined as $M = V_{sh}/C_s$ in the frame of the upstream plasma. As displayed in Fig. 4a, the Mach number for expansion shocks is seen to increase with increasing Γ up to a maximum of ∼1.6 for Γ = 100. Simulations with an increased Γ up to 500 show only a fractional increase in M up to

1.66 showing a clear saturation of the Mach number. Achieving higher Mach numbers is possible in the driven cases as seen in Fig. 4b displaying the Mach number and center-of-mass shock velocity versus V_d. Calculating the Mach number in the driven cases involves a shift to the upstream frame of reference, therefore $M = (V_{sh,cen} + V_d/2)/C_s$. It is clear from this plot the peak Mach number of 3.37 is much higher than in the expansion shock case. Due to their higher Mach numbers, driven shocks are more attractive from an ion acceleration point of view since the shock is able to reflect ions to higher energies for a given temperature of electrons.

Plasma Heating

A shock wave also has the capability to dissipate energy through heating of the electrons and ions of the plasma. This is possible through streaming instabilities inside the shock transition layer where there is strong mixing of the upstream and downstream plasmas. For the conditions of $v_{the} > v_{sh} > C_s$ and $T_e >> T_i$ which are clearly satisfied here, the turbulent modes created within the shock layer that ultimately transfer energy from waves to particles are related to a broad spectrum of ion waves [31]. A detailed description of these microturbulent plasma processes is quite complex and beyond the focus of the current study. However, the macroscopic result of proton and electron heating due to this turbulence as well as proton trapping in subsequent waves behind the shock is an observable in the simulations and is summarized for the driven shock case in Fig. 5. A zoomed in view of the proton and electron phase spaces for the case of $V_d = 0.12c$ is shown in Fig. 5a and b respectively. The downstream side of the shock ($\sim$640 (c/ω_p)) in both the proton and electron phase spaces show a clear broadening of the distribution function with respect to that in the upstream. Though neither of the distributions are Maxwellian, an approximate temperature has been extracted by measuring the V_{FWHM} of the distributions and relating it to the V_{th} of a Maxwellian distribution.

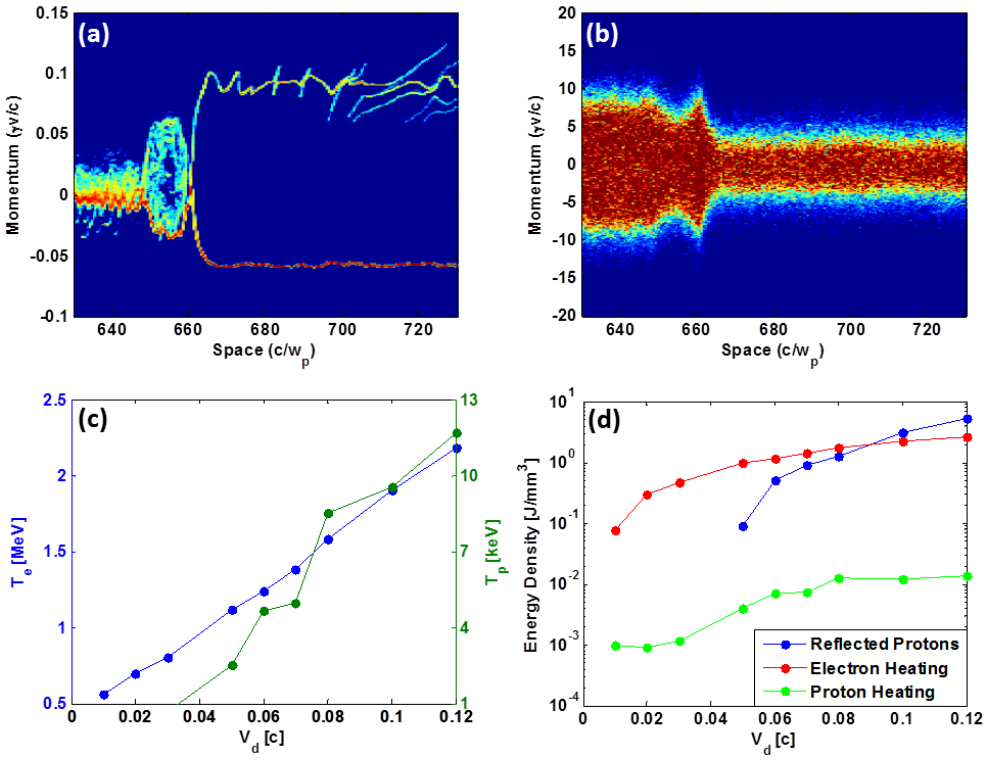

FIGURE 5. Proton (a) and electron (b) longitudinal phase spaces for $V_d = 0.12c$. Approximate downstream temperatures of the protons (green line) and electrons (blue line) versus drive velocity, V_d (c). Energy density in J/mm^3 contained in the heated protons (green line), the reflected protons (blue line), and the heated electrons (red line - compared to initial energy density) (d).

The heated proton and electron temperatures for the driven shock case (initial $T_e = 511$ keV, $T_i = 10$ eV) is plotted versus V_d in Fig. 5c. The heated electron temperature is seen to increase linearly from its initial 511 MeV to a peak of 2.2 MeV as V_d increases to 0.12c. On the other hand, the protons do not show any appreciable heating until V_d reaches

0.05c, the onset of reflection. This seems to be consistent with the idea that proton heating and proton reflection both have their origin in interaction with a moving potential. In the proton reflection case, the moving potential is simply the front of the shock which is fairly monotonic. For protons that traverse through the shock, they experience the accelerating fields from a broad spectrum of excited ion waves that exist in the previously mentioned turbulence.

Fig. 5d is a logarithmic plot of the partition of energy density dissipated through the mechanisms mentioned : proton heating (green line), electron heating (red line), and proton reflection (blue line). Since the protons are only heated to keV levels, the amount of energy they contain is on the order of mJ/mm^2 which is very small compared to the other two mechanisms. However, the energy contained in the protons that are reflected from the shock (calculated as the number of reflected particles times their mean energy) is significant and reaches $\sim$5 J/mm^3 for a V_d of 0.12c corresponding to a reflection efficiency of 28% and a reflected energy of 11.6 MeV. Last, the energy increase in the electrons due to heating is also very significant having values on the J/mm^3 level.

ION ACCELERATION AND LASER DRIVEN SHOCKS

From the point of view of SWA of ions, it is of great interest to decipher what parameters affect the final velocity of protons reflected from the shock wave. According to Eq. 1, this depends strongly on the shock velocity. Here, the interaction considered is a high power laser pulse incident upon an overcritical plasma surface. At the critical plasma density, n_{cr}, part of the laser light is absorbed and part is reflected which exerts a radiation pressure pushing the plasma backwards [32]. Therefore, the laser pulse not only heats up the plasma electrons, both at the critical surface and through the underdense plasma, but also drives the surface back at the hole boring velocity. This speed at which this ion front moves can be calculated by equating the momentum flux of the protons with the pressure of the laser resulting in [14] :

$$\frac{V_{hb}}{c} = \sqrt{\frac{n_{cr}}{n_p}\frac{Zm_e}{M_i}a_o^2} \tag{5}$$

where n_p is the peak plasma density, c is the speed of light and a_o is the normalized vector potential of the laser. This velocity at which the plasma is moving near the front of the laser can be compared to the V_d of the halfplane simulations, therefore it is expected that the shock velocity will scale favorably with the a_o of the laser.

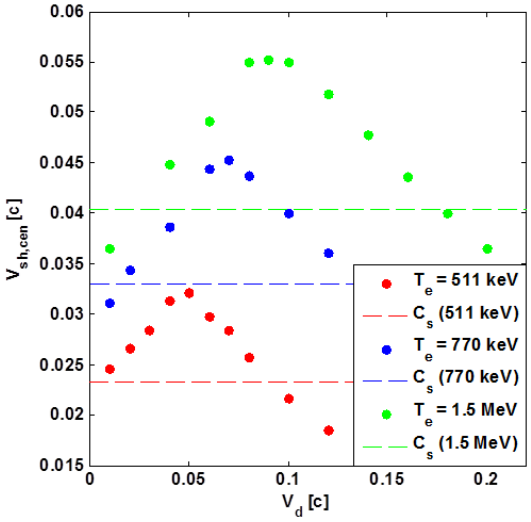

FIGURE 6. The shock velocity in the center-of-mass frame, $V_{sh,cen}$, plotted versus drive velocity, V_d, for the three electron temperatures : T_e = 511 keV (red dots), T_e = 1 MeV (blue dots), and T_e = 1.5 MeV (green dots). These values are compared to the sound speed, C_s, for each temperature which is shown by the dashed line in its respective color.

The shock velocity should also depend on the temperature of the plasma electrons which is related to the sound speed. This can be seen in Fig. 6 where the velocity of the shock in the center-of-mass frame, $V_{sh,cen}$, is tracked versus V_d for three different electron temperatures: T_e = 511 keV (red dots), T_e = 1 MeV (blue dots), and T_e = 1.5 MeV (green dots). Also shown on the plot are the sound speeds for each electron temperature represented by the dashed line

in their respective color. One can see that the cases of T_e = 1 MeV and 1.5 MeV have the same functional dependence of 511 keV as previously shown. V_{sh} is seen to increase with V_d up to a maximum which corresponds to the onset of significant ($\sim$1-2 percent) reflection of protons and then decreases. These dynamics are closely related to the sound speed in each case. First, the drive velocity at which $V_{sh,cen}$ is a maximum, $V_{d,peak}$, roughly increases proportionally with the sound speed ($V_{d,peak}/C_s \sim 2.15$ for each case). Second, for the vast majority of the data, $V_{sh,cen}$ is always faster than C_s and has a maximum value in each case of approximately $1.37C_s$. These results show that the dynamics of shock waves are strongly dependent on the temperature of the electrons of the plasma in which it is propagating and the velocity scales favorably with the acoustic sound speed. The temperature of the electrons in turn will depend in a complicated manner on the laser pulse duration, peak intensity, polarization, and plasma density profile. In this wide variety of conditions, the electron temperature can have a number of different dependencies on the peak a_o of the laser depending on the specific heating mechanism [14, 32, 33].

CONCLUSION

The basic physics of shock wave formation and propagation, and dissipation through plasma heating and ion reflection has been studied via 1D OSIRIS simulations for the interaction of two semi-infinite plasmas. For the cases of initially stationary plasmas (labeled "expansion shocks"), it is observed that the expansion of one dense plasma into a more rarefied one can cause the formation of an ion acoustic wave at smaller density ratios and a shock wave at larger density ratios. Associated with the shock wave is a spike in the proton density as well as the longitudinal electric field which is capable of reflecting up to 100% of the upstream ions, though this value never reaches above $\sim$2% of the downstream density. If the plasmas are collided with an initial velocity, V_d (called "driven shocks"), similar dynamics are observed even with equal initial densities in the two plasmas. In this case, the velocity of the shock in the center-of-mass frame, $V_{sh,cen}$, is lower bounded by the sound speed, C_s, and is seen to increase with V_d up to the point where significant ion reflection begins. Further increase in V_d increases the amount of reflected ions thus dissipating energy from the shock and lowering $V_{sh,cen}$.

From a particle acceleration standpoint, driven shocks are advantageous in peak proton reflection ($\sim$40% versus $\sim$2%) and peak Mach number (3.7 versus 1.9). For achieving these high energy reflected ions in the driven case, two parameters are highlighted which are shown to increase the speed of the shock : electron temperature and initial drift velocity. To zeroth order, the driven shock case is compared with laser driven shocks due to the pushing on the overcritical surface by the laser pulse at the hole boring velocity. The main conclusions from this simple comparison are to optimize the laser pulse and plasma density profile to achieve efficient heating of the electrons and maximum hole boring velocity. There are many refinements of halfplane simulations that could more closely model the shock wave dynamics in the laser driven case : plasmas with finite longitudinal extent, plasmas driven with V_d and a $\Gamma \neq 1$, the study of shock propagation up and/or down a density gradient, etc. Finally, the true applicability of these ideas to the laser driven case can only be tested using 2D or 3D simulations where the interaction of the high power laser with varying plasma density profiles provides a more realistic electron distribution and plasma profile.

ACKNOWLEDGMENTS

Work supported by DOE Grant DE-FG02-92-ER40727, NSF grant PHY-0936266. The authors would also like to thank Frank Tsung and Ben Winjum for their guidance and support in running OSIRIS.

REFERENCES

1. D. Haberberger, et al., *Nature Phys.* **8**, 95 (2012).
2. E. L. Clark, et al., *Phys. Rev. Lett.* **84**, 670 (2000).
3. R. A. Snavely, et al., *Phys. Rev. Lett.* **85**, 2945 (2000).
4. T. E. Cowan, et al., *Phys. Rev. Lett.* **92**, 204801 (2004).
5. M. Borghesi, et al., *Phys. Plasmas* **9**, 2214 (2002).
6. S. V. Bulanov, T. Z. Esirkepov, V. S. Khoroshkov, A. V. Kuznetsov, and F. Pegoraro, *Phys. Lett. A* **299**, 240 (2002).
7. U. Linz, and J. Alonso, *Phys. Rev. STAB* **10**, 094801 (2007).
8. I. Spencer, et al., *Nucl. Instrum. Methods B* **183**, 449 (2001).
9. K. Krushelnick, et al., *IEEE Tran. Plasma Sci.* **28**, 1110 (2000).

10. M. Roth, et al., *Phys. Rev. Lett.* **86**, 436 (2001).
11. A. Noda, et al., "LASER ION PRODUCTION AS THE INJECTOR FOR CANCER THERAPY SYNCHROTRON," in *Proceedings of* LINAC*2002, Gyeongju, Korea*, 2002, p. 644.
12. J. Fuchs, et al., *Nature Phys.* **2**, 48 (2006).
13. L. Robson, et al., *Nature Phys.* **3**, 58 (2007).
14. S. C. Wilks, and W. L. Kruer, *IEEE J. Quan. Elec.* **33**, 1954 (1997).
15. B. M. Hegelich, et al., *Nature* **439**, 441 (2006).
16. H. Schwoerer, et al., *Nature* **439**, 445 (2006).
17. C. Palmer, et al., *Phys. Rev. Lett.* **106**, 014801 (2011).
18. Z. Najmudin, et al., *Phys. Plasmas* **18**, 056705 (2011).
19. A. Macchi, S. Veghini, T. V. Liseykina, and F. Pegoraro, *New J. Physics* **12**, 045013 (2010).
20. A. Henig, et al., *Phys. Rev. Lett.* **103**, 245003 (2009).
21. F. Pegoraro, and S. V. Bulanov, *Phys. Rev. Lett.* **99**, 065002 (2007).
22. O. Adriani, et al., *Science* **332**, 69 (2011).
23. R. Z. Sagdeev, and C. F. Kennel, *Sci. Am.* **264**, 106 (April 1991).
24. R. A. Fonseca, et al., *Lec. Not. Comput. Sci.* **2331**, 342 (2002).
25. G. Sarri, M. E. Dieckmann, I. Kourakis, and M. Borghesi, *Phys. Rev. Lett.* **107**, 025003 (2011).
26. P. Mora, *Phys. Rev. Lett.* **90**, 185002 (2003).
27. J. Denavit, *Phys. Fluids* **22**, 1384 (1979).
28. F. Chen, *Introduction to Plasma Physics and Nuclear Fusion*, Plenium Press, New York, 1984.
29. J. D. Huba, *NRL Plasma Formulary*, Naval Research Laboratory, Washington DC, 2011.
30. L. Spitzer, *Physics of Fully Ionized Gases*, Interscience, New York, 1962.
31. D. A. Tidman, and N. A. Krall, *Shock Waves in Collisionless Plasmas*, Wiley-Interscience, New York, 1971.
32. W. L. Kruer, *The Physics of Laser Plasma Interactions*, Westview Press, Boulder, Colorado, 2003.
33. F. Tsung, S. Y. Tochitsky, D. J. Haberberger, W. B. Mori, and C. Joshi, *J. Plasma Phys.* p. Published Online (2012).